Current **A**pplied **S**cience and **T**echnology e-ISSN: 2586-9396

Curr. Appl. Sci. Technol. 2026, Vol. 26 (No. 1), e0264784

Research article

Tailoring ZnO Nanostructures through Precursor Concentration and Hydrothermal Duration: A Pathway to Efficient Solar Water Splitting

Phanlapa Borklom[1], Narathon Khemasiri[2], Sukittaya Jessadaluk[1], Prapakorn Rattanawarinchai[1], Navaphun Kayunkid[1]*, Sakon Rahong[1], Adirek Rangkasikorn[1], Supamas Wirunchit[1], Annop Klamchuen[2] and Jiti Nukeaw[1]

[1]College of Materials Innovation and Technology (CMIT), King Mongkut's Institute of Technology Ladkrabang, Bangkok, Thailand
[2]National Nanotechnology Center (NANOTEC), National Science and Technology Development Agency (NSTDA), Pathum Thani, Thailand

Received: 27 September 2024, Revised:17 January 2025, Accepted: 5 February 2025, Published: 23 June 2025

Abstract

This work investigated the formation of ZnO nanostructures on ITO substrates prepared by self-seeding hydrothermal synthesis for photoelectrochemical (PEC) water splitting applications. The hydrothermal parameters, precursor concentration and hydrothermal time, were varied to explore their influences on ZnO crystallinity, morphology, and PEC performance. The combinations of X-ray diffraction and field emission scanning electron microscopy revealed highly oriented ZnO nanostructures with diverse morphologies, including small granules, nanorods, dense films, and hexagonal platelets. Topographic profiling of the morphological parameters revealed complex relationships between synthesis conditions and nanostructure characteristics, highlighting the importance of considering aggregation phenomena in substrate-based growth. This aggregation led to deviations from conventional crystal growth theory predictions, particularly for grain density and diameter evolution. PEC performance evaluation identified ZnO nanorods as the optimal morphology, exhibiting a photocurrent density of 0.182 mA/cm² at 0 V vs. Ag/AgCl. Further enhancement was achieved by decorating ZnO nanorods with CdS nanoparticles, resulting in a six-fold increase in photocurrent density (1.2 mA/cm²). This improvement is attributed to expanded light absorption and improved charge separation at the CdS/ZnO interface. Our findings demonstrate the potential of rationally designed ZnO-based nanostructures in the advancement of solar-driven water splitting technologies and provide valuable insights for optimizing PEC systems through precise control of hydrothermal synthesis parameters, consideration of substrate-induced aggregation, and strategies for photoelectrochemical (PEC) water splitting applications.

Keywords: ZnO nanostructures; hydrothermal synthesis; PEC water splitting; CdS/ZnO nanorods; photoanode

*Corresponding author: E-mail: navaphun.ka@kmitl.ac.th
https://doi.org/10.55003/cast.2025.264784

1. Introduction

Zinc oxide (ZnO) has gained significant attention in the realm of material science and nanotechnology due to its various applications, e.g., optoelectronics, energy harvesting, chemical and biological sensing, environmental remediation, as well as medical diagnosis (Kumar & Kim, 2012; Khan et al., 2021; Preeti et al., 2023; Ahmad & Lee, 2024; Hussain et al., 2024; Pagano et al., 2024; Palem et al., 2024; Worasawat et al., 2019). The ability to control the growth of ZnO nanostructures, e.g., particles, rods, and platelets, with precision holds paramount importance for tailoring their properties to specific applications (Siriphongsapak et al., 2020; Chibac-Scutaru et al., 2024; Joongpun et al., 2024). Among several preparation processes to obtain high quality ZnO, hydrothermal synthesis has emerged as a versatile and effective technique for the fabrication of ZnO nanostructures with controlled morphologies and properties.

Hydrothermal synthesis offers a unique platform for manipulating the growth kinetics and morphological evolution of ZnO nanostructures via adjustment of the growth parameters, e.g., temperature, pressure, precursor concentration, pH, and reaction time (Wasly et al., 2018; Leite et al., 2024). Such parameters play pivotal roles in determining the crystallinity, morphology, size, and optical properties of the synthesized ZnO nanostructures (Polsongkram et al., 2008; Zhang et al., 2011; Liang et al., 2014). Within the hydrothermal synthesis parameters, precursor concentration and hydrothermal duration are primarily and precisely controlled since they have a direct influence on the mechanism of crystal growth. The precursor concentration plays a crucial role in determining the nucleation rate, growth kinetics, and crystallographic orientation of ZnO nanostructures (Mustafa et al., 2017). Furthermore, the synthesis time governs the extent of nucleation and growth, influencing the size distribution, aspect ratio, and structural defects of the ZnO nanostructures (Georgiou et al., 2009; Holi et al., 2016). By varying the precursor concentration and synthesis time, morphological tailoring of the synthesized ZnO nanostructures can be achieved (Cho et al., 2011; AL-Zahrani et al., 2020).

Among the applications utilizing nanostructured ZnO, photoelectrochemical (PEC) water splitting, an electrochemical process driven by solar energy, holds immense promise for producing hydrogen as a clean and renewable fuel (Galdámez-Martínez et al., 2020). To obtain an efficient PEC water splitting device, the development of high-performance photoelectrodes plays a crucial role in facilitating the photoelectrochemical conversion of water into hydrogen and oxygen (Wang et al., 2024). ZnO has emerged as a compelling candidate for photoelectrochemical anodes owing to its outstanding electronic properties, low manufacturing cost, and exceptional chemical and environmental stability. Moreover, the morphology and surface characteristics of ZnO nanostructures exert profound influences on their photoelectrochemical performance, making them highly tunable platforms for efficient water splitting applications (El ouardi et al., 2024). Therefore, the ability to control the formation of ZnO to obtain desired nanostructures becomes key to achieving high-efficiency PEC water splitting devices.

2. Materials and Methods

This work, as shown in Figure 1, was separated into two parts: (i) the influence of precursor concentration and synthesis time on the morphological formation of ZnO on substrate via self-seeding hydrothermal synthesis and (ii) the utilization of different ZnO nanostructures as a photoanodes for PEC water splitting application. In the first part, the synergetic effects of precursor concentration and synthesis time are illustrated by topographic profiles of

morphological parameters, e.g., density, diameter, height, and aspect ratio of ZnO formed on the substrate. The role of precursor concentration and synthesis duration on ZnO formation were discussed based on the mechanism of crystal growth. The second part presents the utilization of different ZnO morphologies as the photoanodes of PEC water splitting cells. The suitable ZnO morphology for such an application was qualitatively examined by generated photocurrent through the photoanode. In addition, the decoration of cadmium sulfide (CdS) nanoparticles on ZnO to form CdS/ZnO heterojunction was applied to the morphology which provided the best PEC performance to illustrate the further enhancement of PEC activity.

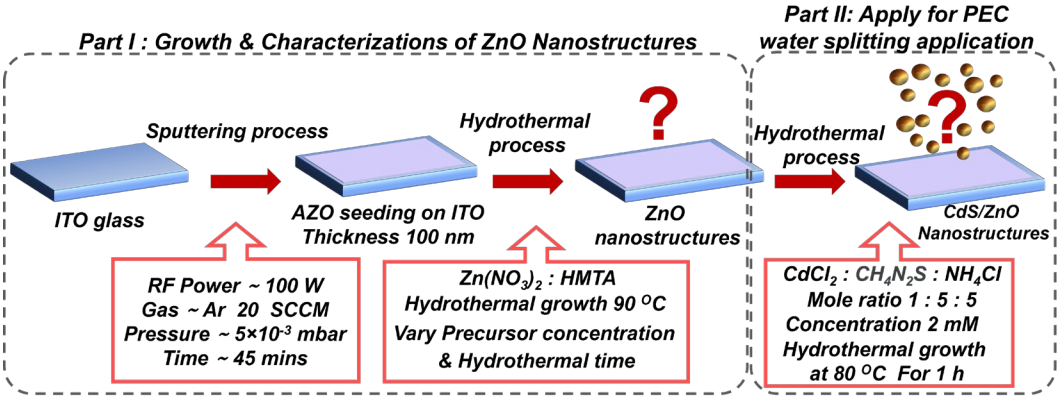

Figure 1. The schematic overview of this work, consisting of Part I: the influence of precursor concentration and synthesis time on the morphological formation of ZnO on substrate via self-seeding hydrothermal synthesis and Part II: the utilization of different ZnO nanostructures as photoanodes for PEC water splitting applications.

2.1 Materials

Zinc nitrate hexahydrate ($Zn(NO_3)_2 \cdot 6H_2O$), hexamethylenetetramine ($C_6H_{12}N_4$) (≥ 99%), and thiourea (CH_4N_2S) (≥ 99%) were purchased from Sigma-Aldrich. Cadmium chloride monohydrate ($CdCl_2 \cdot H_2O$) (99.5-102.0%) was purchased from Himedia Laboratories. Ammonium chloride (NH_4Cl) (99.9%) was purchased from VWR Chemicals BDH. All materials in this experiment were used without additional purification.

2.2 Fabrication of ZnO nanostructures via self-seeding hydrothermal synthesis

2.2.1 Preparation of aluminum doped ZnO (AZO) seeding layer

In this work, ZnO nanostructures were prepared on an aluminum doped ZnO (AZO) thin film. AZO layer provides a seeding template for the growth of ZnO and is a buffer layer between ZnO and ITO electrode used in further electrochemical measurements. Moreover, the AZO layer was also employed to avoid lattice mismatch between cubic-based ITO and hexagonal-based ZnO. To obtain the AZO layer on the ITO substrate, 2×2 cm^2 ITO substrates were initially cleaned in an ultrasonic bath with acetone, isopropyl alcohol and deionized water, respectively. Then, the AZO layer was deposited on the ITO by RF magnetron sputtering using a AZO ceramic target (ZnO/Al_2O_3 : 98/2 %wt). The sputtering

pressure was maintained at 5×10^{-3} mbar, with pure argon (Ar) at the flow rate of 20 sccm. The applied sputtering power was fixed at 100 W for deposition time of 45 min. Finally, the AZO thin film with the thickness of 100 nm was obtained on ITO substrate.

2.2.2 Growth of ZnO nanostructures on AZO thin film

ZnO nanostructures were grown on AZO seeding template via hydrothermal synthesis. The AZO template was treated by reactive-ion etching (RIE) at 30 W for 10 min to remove organic residues and reduce surface roughness of the AZO films. Then, the AZO seeding substrate was submerged in a 100 mL of nutrient solution consisting of zinc nitrate hexahydrate ($Zn(NO_3)_2\bullet 6H_2O$) and hexamethylenetetramine ($C_6H_{12}N_4$), with varied precursor concentrations of 10, 20, 40, 60, 80 and 100 mM. The nutrient solutions were meticulously prepared at room temperature and stirred overnight. The hydrothermal temperature was consistently maintained at 90°C for growth durations of 0.5, 1, 2, 4 and 6 h, respectively, to facilitate the growth of ZnO NRs on AZO/ ITO substrate. The hydrothermal process adheres to specific chemical equations governing the reactions involved in the synthesis as follows:

$$Zn(NO_3)_2 \rightarrow Zn^{2+} + 2NO_3^- \quad (1)$$

$$C_6H_{12}N_4 + 6H_2O \rightarrow 6HCHO + 4NH_3 \quad (2)$$

$$NH_3 + H_2O \leftrightarrow NH_4^+ + OH^- \quad (3)$$

$$Zn^{2+} + 2OH^- \leftrightarrow ZnO_{nuclei} + H_2O \quad (4)$$

After finishing the growth processes, all prepared samples were rinsed with deionized water and ethanol and finally dried in the air at 80°C. Finally, the various nanostructures of ZnO were obtained on the substrate.

2.3 Characterizations

The morphology of the ZnO nanostructures was characterized by field emission scanning electron microscope (FESEM, Hitachi SU8030) with an acceleration voltage of 10 kV. The crystalline formation was determined by X-ray diffraction (XRD, Smart Lab, Rigaku) with CuK_α radiation. The apparent crystalline size was calculated by Scherrer's equation without the consideration of micro-strain in the sample. The photoelectrochemical (PEC) activity of 1x1 cm^2 ZnO photoanodes was evaluated by using a three-electrode electrochemical cell (Methrom, PGSTAT 302N) in 0.25 M sodium sulphite (Na_2SO_3) under AM 1.5 G solar irradiation at 100 mW/cm^2 (Solar light, XPS-300 series). Commercial Ag/AgCl and Pt sheet were employed as the reference and counting electrodes, respectively. The ZnO photoanode was stimulated using front illumination. The chronoamperometry test (I-t) analysis was measured without bias potential (0 V versus Ag/AgCl).

2.4 Fabrication of CdS nanoparticles on ZnO surface for improvement of PEC activity

After obtaining the suitable ZnO morphology for PEC water splitting applications, the decoration of CdS nanoparticles onto the ZnO surface was employed to enhance PEC activity via the formation of CdS/ZnO junction. CdS nanoparticles were deposited onto the surface of ZnO NRs via hydrothermal synthesis. The ZnO nanostructure was immersed into 30 mL of formulated growth solution, containing $CdCl_2$: CH_4N_2S : NH_4Cl, at a molar ratio of 1:5:5 mM and $CdCl_2$ concentration of 2 mM. The hydrothermal synthesis was conducted at a controlled temperature of 80°C for 1 h. Subsequently, CdS/ZnO sample was rinsed with deionized water and ethanol before finally dried in ambient air at 80°C.

3. Results and Discussion

X-ray diffraction analysis shown in Figure 2 reveals the crystalline structure and orientation of ZnO samples prepared via seed-assisted hydrothermal synthesis with varying precursor concentrations and hydrothermal times. All samples exhibit a dominant diffracting peak at 34.5°, corresponding to the (002) plane of hexagonal ZnO (JCPDS:39-1451) (Wei et al., 2017). This confirms the formation of highly oriented ZnO nanostructures growing perpendicular to the substrate. The absence of peak shifts suggests that precursor concentration and hydrothermal time primarily influence ZnO formation, without additional factors like stress-induced crystallization (Chen et al., 2005). Increasing either parameter enhances the peak intensity, indicating more ZnO grown on the substrate. However, excessively high precursor concentration (~100 mM) weakens the peak intensity, potentially due to growth-induced defects (Kumari & Kar, 2018).

To reveal the influence of precursor concentration and hydrothermal time on crystalline size, the width of the (002) diffracting peak in each preparation condition was employed to calculate the crystallite size of ZnO along the [002] direction via the Scherrer equation (Khan et al., 2021) without consideration of micro-strain induced broadening. The apparent crystallite size along the [002] direction of ZnO samples obtained from all preparation conditions are illustrated in Figure 2e and alternatively presented as topographic profile in Figure 2f to represent the overall influences due to both precursor concentration and hydrothermal time. In Figure 2e and 2f, the crystallite size of all precursor concentrations tends to rapidly increase as a function of time then reaches to the saturated size after 4 h of synthesizing time. The observed trend in crystallite size evolution along the [002] direction can be attributed to the classical crystal growth mechanisms governed by Ostwald ripening and the system's thermodynamic driving forces. Initially, the rapid increase in crystallite size occurs due to the high supersaturation of Zn^{2+} species in the solution, which promotes preferential growth along the c-axis ([002] direction) owing to ZnO's wurtzite crystal structure. This preferential growth is facilitated by the polar nature of the (002) face, which has a higher surface energy compared to other crystallographic planes. As the reaction progresses, the growth rate gradually decreases and approaches saturation due to several factors: (i) the depletion of Zn^{2+} ions in the solution reduces the chemical potential difference driving the crystal growth, (ii) the decrease in surface energy of larger crystals diminishes the thermodynamic driving force for further growth, and (iii) the establishment of a dynamic equilibrium between dissolution and recrystallization processes characteristic of Ostwald ripening (Polsongkram et al., 2008; Cho et al., 2011; Wasly et al., 2018). This behavior follows a typical crystal growth profile where the final plateau represents a metastable state where further significant changes in crystallite size are kinetically limited under the given hydrothermal conditions.

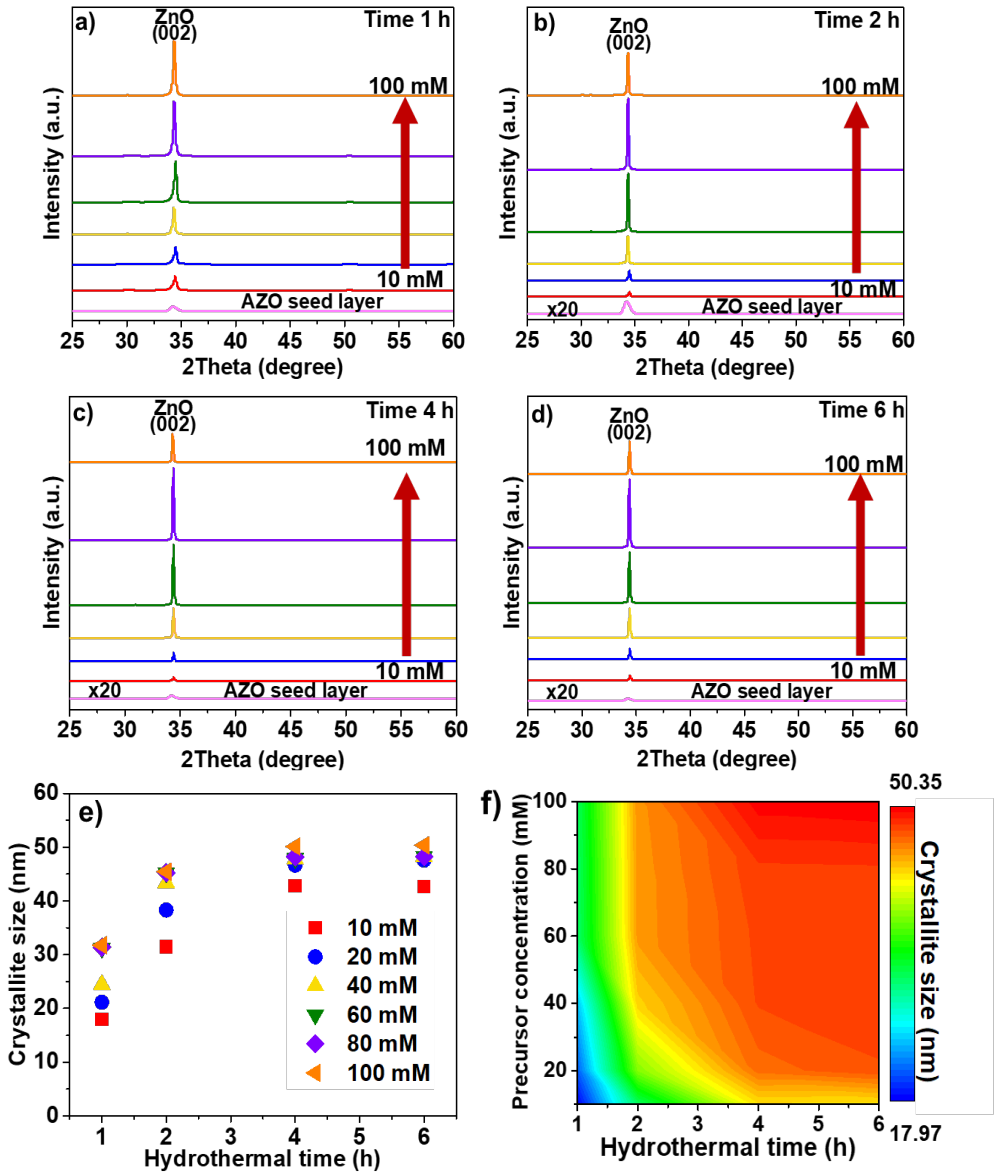

Figure 2. XRD diffractograms of ZnO nanostructures on AZO/ITO substrates using hydrothermal times of a) 1 h, b) 2 h, c) 4 h, and d) 6 h with different precursor concentrations from 10 mM to 100 mM, e) Variation of crystallite size obtained from different precursor concentrations as a function of hydrothermal time and f) Topographic contours of crystallite size collected from ZnO nanostructures on AZO/ITO substrates with different precursor concentrations and hydrothermal times.

Furthermore, the higher precursor concentration was used, and the larger crystalize was obtained. The observed correlation between precursor concentration and apparent crystallite size of ZnO can be explained through nucleation and growth kinetics. At higher initial Zn^{2+} precursor concentrations, the increased supersaturation ratio provides a stronger thermodynamic driving force for crystal growth (Cho et al., 2011). This enhanced driving force manifests in two key aspects: (i) it increases the chemical potential gradient between the solution and crystal surface, accelerating the diffusion and incorporation of growth units onto the crystal faces, and (ii) it provides sufficient ion availability to sustain growth over extended periods. In addition, the higher concentration of precursor species increases the probability of successful molecular collisions and attachments at the crystal surface. This leads to more effective incorporation of growth units into the crystal lattice, particularly along the energetically favorable [002] direction. The abundance of available Zn^{2+} ions in concentrated solutions also supports the formation of larger critical nuclei during the initial nucleation stage, which serve as more stable templates for subsequent crystal growth.

However, it is important to note that this concentration-dependent size increase typically exhibits a saturation behavior beyond a critical concentration, where further increases in precursor concentration may not significantly affect the final crystal size due to factors such as solution stability limits and the kinetics of surface integration.

Field emission scanning electron microscopy (FE-SEM) was utilized to investigate the influence of hydrothermal parameters on the morphological formation of ZnO nanostructures. The bright-field micrographs illustrated in Figure 3 reveal diverse hexagonal morphologies, including small granules, nanorods, dense films, and large hexagonal platelets, which were obtained by varying precursor concentrations and hydrothermal durations. Specifically, low precursor concentration and short hydrothermal time result in small, isolated granules. Conversely, increasing both parameters promotes the formation of thick, overlapping platelets. Notably, optimized hydrothermal conditions enable the controlled growth of nanorods. This demonstrated control over ZnO morphology through tailored hydrothermal parameters highlights its potential for application-specific design. By optimizing growth conditions, the unique properties of different ZnO structures can be harnessed for targeted applications.

The topographic profiles shown in Figure 4, representing key morphological parameters of ZnO such as grain density, average diameter, average length, and aspect ratio, were derived from FESEM images obtained at different precursor concentrations and synthesis duration. These profiles utilize a color scale to quantitatively represent the parameters' values. The effects of precursor concentration and synthesis time on each morphological parameter are analyzed as follows:

Grain density: As shown in Figure 4a), contrary to conventional crystal growth theory, which predicts increased nucleation and density at higher precursor concentrations (Promnimit et al., 2013), our results reveal more complex relationships. The highest density is observed at low precursor concentrations and short synthesis times, with a decrease at higher concentrations and longer synthesis times. This unexpected trend can be attributed to a synergistic effect between precursor concentration and synthesis time. The increment of precursor concentration initially promotes nucleation of ZnO nuclei, but within a confined area, leading to the formation of closely spaced ZnO nuclei. The prolonged synthesis time facilitates the growth along the a-plane of ZnO, inducing the aggregation of adjacent nuclei and effectively reducing the overall grain density (Almamari et al., 2022). This interplay between nucleation and growth kinetics highlights the importance of carefully balancing synthesis parameters to control ZnO nanostructure density.

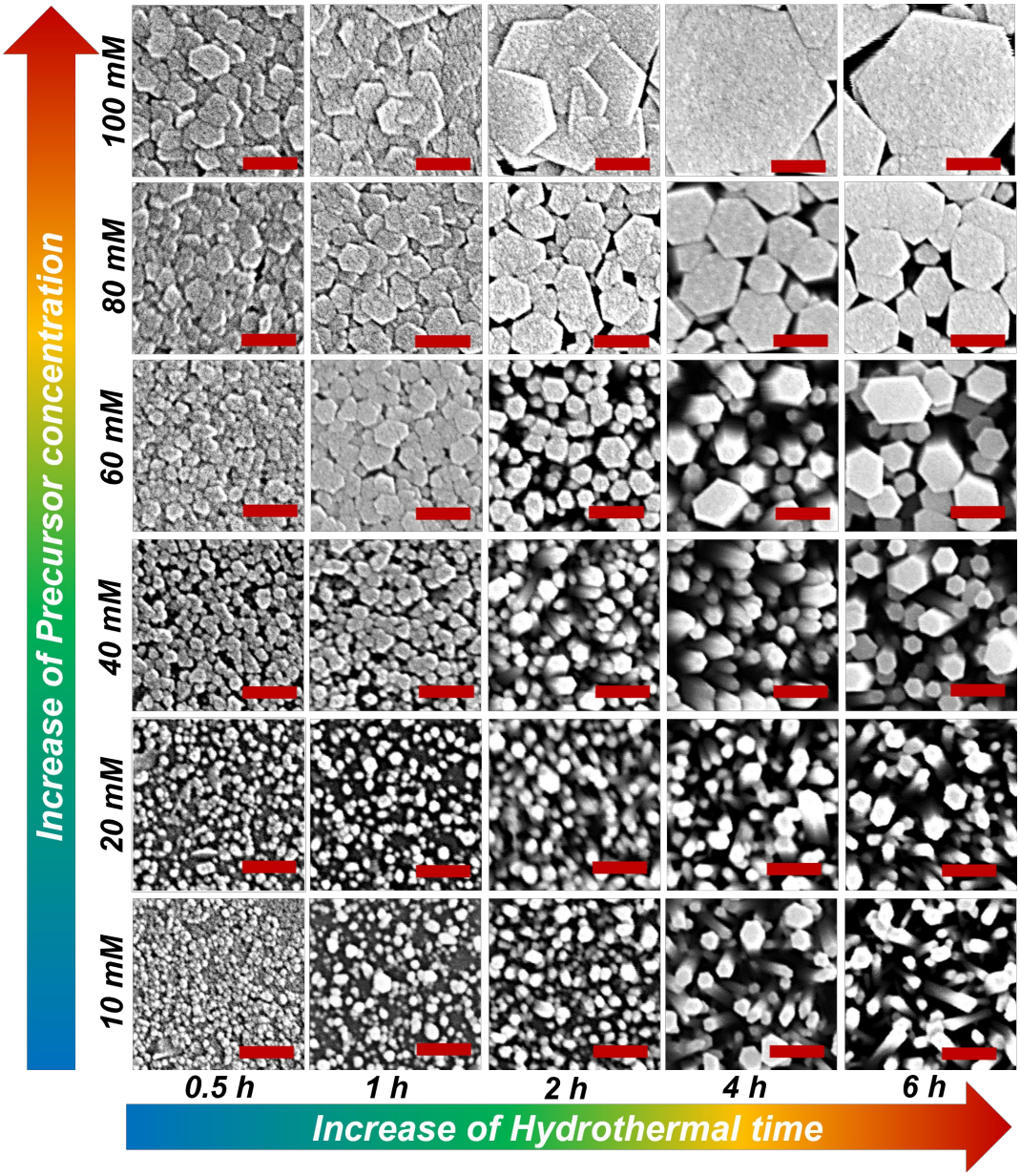

Figure 3. SEM images presenting the different formation of ZnO nanostructures on AZO/ITO substrates obtained from different precursor concentrations and hydrothermal times (scale bar in the figure represents the dimension of 200 nm).

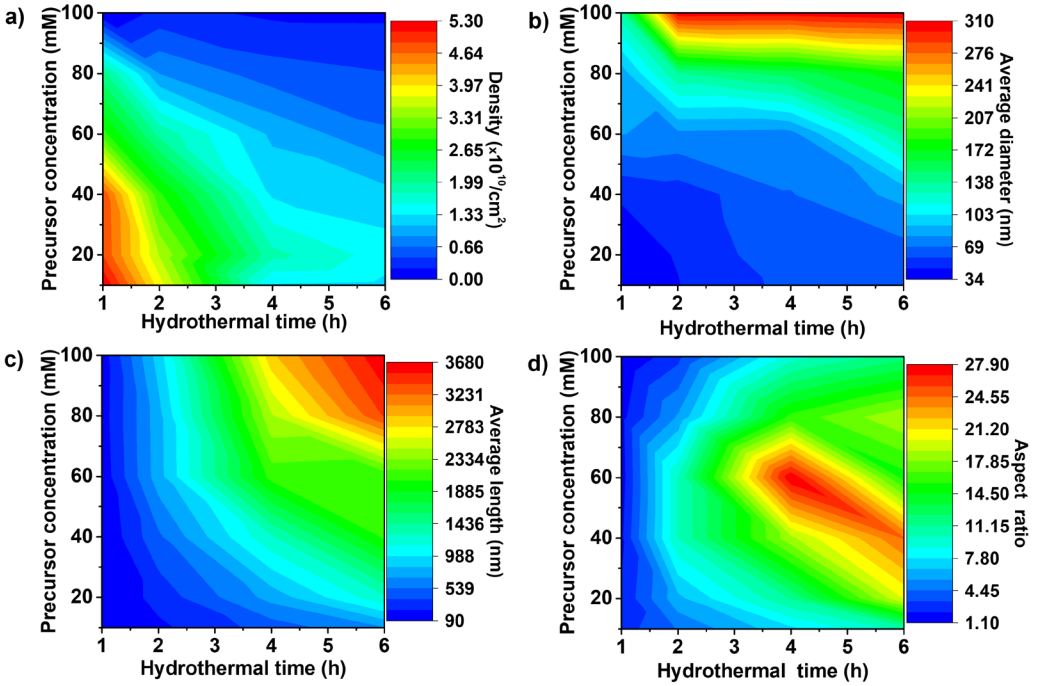

Figure 4. Topographic contours of morphological parameters a) density, b) average diameter, c) average length, and d) aspect ratio, collected from ZnO nanostructures on AZO/ITO substrates with different precursor concentrations and hydrothermal times

Grain Diameter: Figure 4b) demonstrates that the largest diameters were achieved at high precursor concentrations, with a significant decrease at lower concentrations. Interestingly, synthesis time shows minimal influence on lateral growth of ZnO. While ZnO growth theory typically associates lateral growth in the (100) plane with synthesis time (Al-Rasheedi et al., 2024), our observations suggest a more significant role for precursor concentration. This unexpected effect likely stems from precursor-induced aggregation of ZnO nanostructures, rather than true lateral growth. Thus, controlling both aggregation of nucleation sites and lateral growth appears to be predominantly influenced by precursor concentration in this system.

Average Length: The results in Figure 4c align with theoretical predictions, showing that both longer synthesis times and higher precursor concentrations lead to increased ZnO nanostructure length (Promnimit et al., 2013). Higher precursor concentrations provide more nutrients during the hydrothermal process, promoting growth along both the c-plane and a-plane. This observation underscores the critical role of nutrient availability in determining the final dimensions of ZnO nanostructures.

Aspect Ratio: The aspect ratio represented in Figure 4d, defined as the ratio of average length (in Figure 4c) to diameter (in Figure 4b), is a crucial parameter influencing the properties and potential applications of ZnO nanostructures, especially, rod-like structure. Our findings indicate that the aspect ratio is maximized at moderate precursor concentrations and extended synthesis duration. This optimal condition strikes a balance between promoting longitudinal growth (020) while minimizing lateral expansion (100) and aggregation between adjacent ZnO crystals (Al-Rasheedi et al., 2024).

These results provide valuable insights into the complex interplay between synthesis parameters and morphology of ZnO nanostructure. By carefully tuning precursor concentration and synthesis time, it is possible to tailor the grain density, dimensions, and aspect ratio of ZnO nanostructures for specific applications. For instance, high-aspect-ratio nanostructures may be preferred for applications requiring large surface areas, such as gas sensing or photocatalysis, while lower aspect ratios might be more suitable for optoelectronic devices (Hassanpour et al., 2017; Sha et al., 2022). Furthermore, the observed deviations from conventional growth theories highlight the importance of considering synergistic effects and secondary growth mechanisms, such as aggregation, in hydrothermal synthesis. These findings contribute to a more nuanced understanding of ZnO nanostructure growth and may inform the development of more precise control strategies for other metal oxide nanostructures synthesized via hydrothermal methods.

The results for the hydrothermal synthesis of ZnO demonstrate that varying precursor concentrations and hydrothermal durations significantly influence ZnO morphology. The study identifies four distinct morphological zones, as illustrated in Figure 5a. High precursor concentrations with short synthesis times produce a dense film morphology (Figure 5a, zone I), while high concentrations combined with longer durations result in large platelets (Figure 5a, zone II). Conversely, low precursor concentrations and short synthesis times lead to a small granular morphology (Figure 5a, zone III), and low concentrations with extended times yield ZnO nanorods (Figure 5a, zone IV). To determine the optimal morphology of ZnO nanostructures for PEC water splitting applications, each ZnO morphology was employed as a photoanode to measure PEC activity via amperometry analysis.

Figure 5b presents the amperometric measurements obtained from ZnO photoanodes with varying morphologies. The results demonstrate a clear correlation between ZnO nanostructure morphology and photocurrent density in photoelectrochemical (PEC) water splitting applications. ZnO nanorods exhibit the highest photocurrent density of $0.182\ mA/cm^2$, followed by large platelets ($0.052\ mA/cm^2$), small granules ($0.041\ mA/cm^2$), and dense films ($0.027\ mA/cm^2$), respectively. The superior performance of the rod-like nanostructures can be attributed to several factors: (i) the increment in the active sites for water oxidation reactions due to the large surface area in nanorod structure and (ii) the efficient charge collection owing to the one-dimensional charge transport in nanorod structure (Lai et al., 2021; Lee et al., 2024).

To further elucidate the relationship between synthesis parameters and PEC performance, a topographic representation of photocurrent density as a function of precursor concentration and hydrothermal duration is presented in Figure 5c. This analysis reveals an optimal regime for high photocurrent generation, corresponding to precursor concentrations between 30 and 60 mM and hydrothermal durations of 2 to 5 h. Correlating these findings with the SEM micrographs in Figure 2 confirms that the highest PEC activity is indeed achieved with ZnO nanorod structures formed under these specific conditions. This alignment of morphological and performance data underscores the critical role of precise synthetic control in optimizing ZnO photoanodes for PEC water splitting.

Although the above results suggest that nanorods are a suitable structure for PEC water splitting, the efficiency is rather low. To further enhance PEC water splitting efficiency, several studies have proposed that the incorporation of CdS nanoparticles onto ZnO nanorods is a promising approach (Hoang et al., 2017; Wei et al., 2017; Kolaei et al., 2022). Therefore, we took the ZnO nanorods that provided the highest PEC activity (synthesized at 40 mM precursor concentration and 4 h hydrothermal duration) and decorated them with CdS nanoparticles via a hydrothermal process.

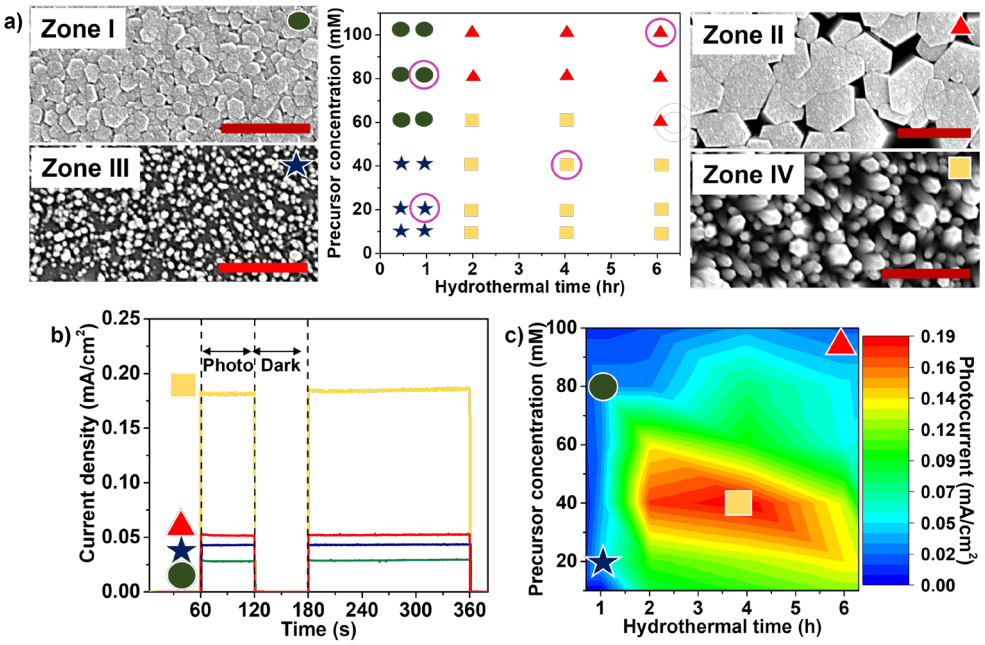

Figure 5. a) Representations of various ZnO morphologies, including dense film (zone I●), hexagonal plates (zone II ▲), small granules (zone III ★), and nanorods (zone IV ■), obtained from varying hydrothermal parameters. b) Amperometric measurements of ZnO photoanodes with different morphologies, and c) Topographic contour of photocurrent obtained from ZnO photoanodes with various precursor concentrations and hydrothermal times (scale bar = 500 nm).

The X-ray diffractogram shown in Figure 6a reveals additional diffraction peaks at 24.9°, 26.7°, 28.4°, and 44.0°, corresponding to the (100), (002), (101), and (102) planes of hexagonal CdS (JCPDS: 41-1049) (Wei et al., 2017). SEM micrographs in Figures 6b and 6c illustrate the morphology of ZnO nanorods and ZnO nanorods decorated with CdS nanoparticles, respectively. The increase in average diameter of the nanorod structure from 70.73 nm (ZnO nanorods) to 129.93 nm (CdS/ZnO nanorods) confirms the successful decoration of CdS nanoparticles on ZnO nanorods.

Figure 7a presents a comparison of photocurrent density response (I−t) curves obtained from ZnO nanorods and CdS/ZnO nanorods photoanodes. The measurement was carried out at open circuit potential with 60-second on−off solar irradiation cycles. The photocurrent densities for the ZnO nanorods and CdS/ZnO nanorods photoanodes are approximately 0.19 and 1.2 mA/cm², respectively. These results indicate that the CdS/ZnO nanorod photoanode delivers a photocurrent density approximately 6 times greater than that of the ZnO nanorods photoanode. Moreover, the photocurrent shows no significant reduction over time, suggesting the stability of CdS/ZnO-nanorods photoanode. Figure 7b illustrates the overall schematic representation of the PEC mechanism utilizing CdS/ZnO nanorods as a photoanode. The significant enhancement in PEC performance can be attributed to several synergistic factors: (i) the increment in photogenerated excitons

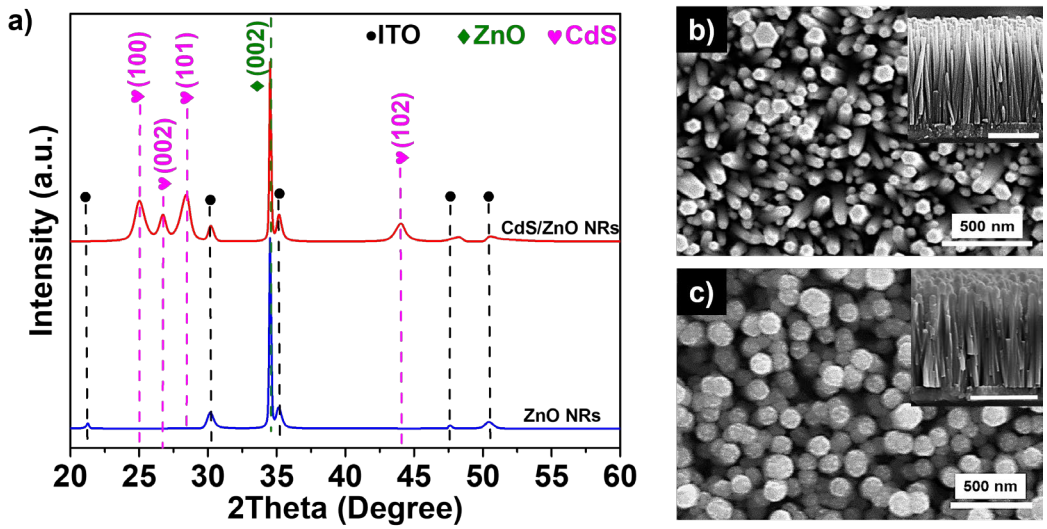

Figure 6. a) XRD diffractograms of ZnO nanorods and CdS/ZnO nanorods on AZO/ITO substrates. The SEM images of b) Bare-ZnO nanorods and c) CdS/ZnO nanorods (inset 6b) and 6c) presenting cross sectional images with the scale bar presenting 1 μm in length).

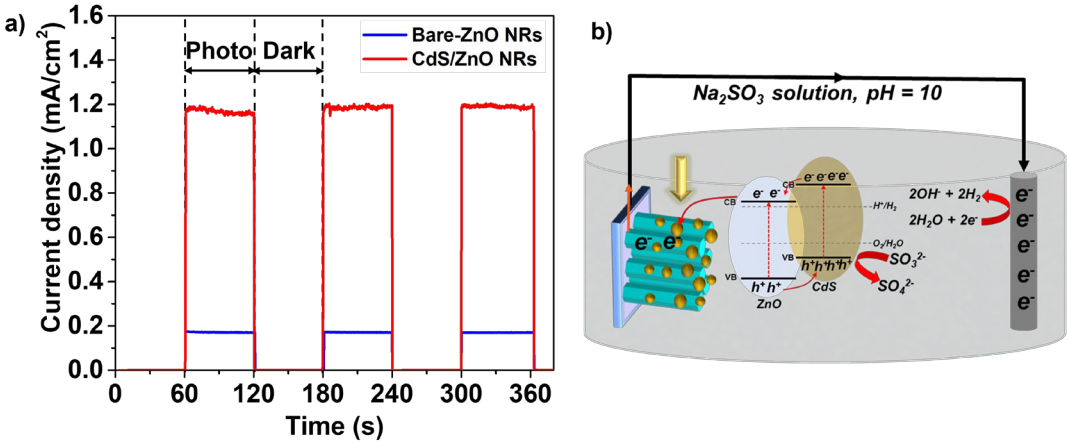

Figure 7. a) Amperometric measurement of ZnO NR and CdS/ZnO NR photoanodes under dark and simulated-solar irradiation at 0 V Vs Ag/AgCl b) Schematic representation of PEC water splitting mechanism utilizing CdS/ZnO NRs as a photoanode.

due to the narrower bandgap of CdS (~2.5 eV) compared to ZnO (~3.2 eV), and (ii) the better charge carrier transfer and longer charge carrier lifetime due to the formation of type II band alignment taken place at the CdS/ZnO interface (Banerjee et al., 2000; Doiphode et al., 2024). The combination of these factors results in more efficient light harvesting, charge separation, and charge transport, leading to the observed six-fold increase in photocurrent density. This significant improvement underscores the potential of carefully designed heterojunction nanostructures in advancing PEC water splitting technology.

4. Conclusions

This study provides comprehensive insights into the hydrothermal synthesis of ZnO nanostructures and their application in photoelectrochemical (PEC) water splitting. The research demonstrates the critical influence of precursor concentration and hydrothermal duration on the morphology, crystallinity, and PEC performance of ZnO nanostructures. XRD analysis confirmed the formation of highly oriented ZnO nanostructures with a dominant (002) plane, indicating growth perpendicular to the substrate. In addition, SEM micrographs revealed diverse ZnO morphologies, including granules, nanorods, dense films, and hexagonal platelets, achievable through the precise control of synthesis parameters. Topographic profiling of morphological parameters (grain density, diameter, length, and aspect ratio) unveiled complex relationships between synthesis conditions and nanostructure characteristics, which often deviated from conventional crystal growth theories due to the aggregation of adjacent ZnO domains. PEC performance evaluation identified ZnO nanorods as the optimal morphology for water splitting applications, exhibiting the highest photocurrent density of 0.182 mA/cm² at 0 V vs. Ag/AgCl. Further enhancement was achieved by decorating the ZnO nanorods with CdS nanoparticles, resulting in a remarkable six-fold increase in photocurrent density (1.2 mA/cm²) compared to bare ZnO nanorods. This research provides not only understanding of ZnO nanostructure growth mechanisms but also valuable insights for optimizing PEC water splitting systems. The demonstrated ability to fine- tune ZnO morphology through hydrothermal synthesis parameters, coupled with strategic heterostructure design, opens new avenues for enhancing the efficiency of solar water splitting technologies.

5. Acknowledgements

This research received funding support from the NSRF via the Program Management Unit for Human Resources & Institutional Development, Research and Innovation grant number B05F640227. The authors acknowledge the facilities and technical assistance from Nanotechnology and Materials Analytical Instrument Service Unit (NMIS) of College of Materials Innovation and Technology, King Mongkut Institute of Technology Ladkrabang

6. Author Contributions

Phanlapa Borklom: designed and performed experimental setup, collected and analyzed experimental results, drafted and wrote the manuscript. Narathon Khemasiri, and Navaphun Kayunkid: suggested the concept idea and experimental method, reviewed and edited the manuscript. Sukittaya Jessadaluk and Prapakorn Rattanawarinchai: supported the experimental setup and data collection. Sakon Rahong, Adirek Rangkasikorn, Supamas Wirunchit, and Annop Klamchuen: extensive suggested the experimental approach, reviewed the manuscript. Jiti Nukeaw: supervised and conceived this project.

7. Conflicts of Interest

The authors declare that there is no conflict of interest in this study.

References

Ahmad, R., & Lee, B.-I. (2024). Facile fabrication of palm trunk–like ZnO hierarchical nanostructure–based biosensor for wide-range glucose detection. *Chemical Engineering Journal,* 492, Article 152432. https://doi.org/10.1016/j.cej.2024.152432

Almamari, M. R., Ahmed, N. M., Holi, A. M., Yam, F. K., Kyaw, H. H., Almessiere, M. A., & Al-Abri, M. Z. (2022). Some distinct attributes of ZnO nanorods arrays: Effects of varying hydrothermal growth time. *Materials,* 15(17), Article 5827. https://doi.org/10.3390/ma15175827

Al-Rasheedi, A., Salwati, A. A., & Aida, M. S. (2024). Growth of variable aspect ratio ZnO nanorods by hydrothermal technique. *Physica Scripta*, 99(6), Article 065996. https://doi.org/10.1088/1402-4896/ad4697

AL-Zahrani, A. A., Zainal, Z., Talib, Z. A., Ngee, J. L. H., Fudzi, L. M., Holi, A. M., & Ali, M. S. (2020). Effect of hydrothermal growth temperature and time on physical properties and photoanode performance of Zno nanorods. *International Journal of Nanoelectronics and Materials*, 13(2), 381-400.

Banerjee, R., Jayakrishnan, R., Banerjee, R., & Ayyub, P. (2000). Effect of the size-induced structural transformation on the band gap in CdS nanoparticles. *Journal of Physics: Condensed Matter*, 12(50), Article 10647. https://doi.org/10.1088/0953-8984/12/50/325

Chen, Y. W., Liu, Y. C., Lu, S. X., Xu, C. S., Shao, C. L., Wang, C., Zhang, J. Y., Lu, Y. M., Shen, D. Z., & Fan, X. W. (2005). Optical properties of ZnO and ZnO: In nanorods assembled by sol-gel method. *The Journal of Chemical Physics,* 123(13), Article 134701. https://doi.org/10.1063/1.2009731

Chibac-Scutaru, A. L., Podasca, V.-E., Dascalu, I. A., Rusu, D., & Melinte, V. (2024). ZnO nanostructures with controlled morphological and optical properties for applications as efficient photocatalyst for malachite green degradation. *Ceramics International,* 50(18), 34291-34303. https://doi.org/10.1016/j.ceramint.2024.06.248

Cho, M. Y., Kim, M. S., Yim, K. G., Lee, D. Y., Kim, J. S., Kim, J. S., & Leem, J. Y. (2011). Effects of precursor concentrations and thermal annealing on ZnO nanorods grown by hydrothermal method. *Journal of Nanoscience and Nanotechnology,* 11(8), 7479-7482. https://doi.org/10.1166/jnn.2011.4783

Doiphode, V., Shinde, P., Punde, A., Shah, S., Kale, D., Hase, Y., Ladhane, S., Rahane, S., Waghmare, A., Bade, B., Rondiya, S., Prasad, M., Patole, S. P., & Jadkar, S. (2024). Solution-processed synthesis of ZnO/CdS heterostructure photoanode for efficient photoelectrochemical water splitting. *Journal of Power Sources*, 609, Article 234712. https://doi.org/10.1016/j.jpowsour.2024.234712

El ouardi, M., El Idrissi, A., Ahsaine, H. A., BaQais, A., Saadi, M., & Arab, M. (2024). Current advances on nanostructured oxide photoelectrocatalysts for water splitting: A comprehensive review. *Surfaces and Interfaces,* 45, Article 103850. https://doi.org/10.1016/ j.surfin.2024.103850

Galdámez-Martínez, A., Bai, Y., Santana, G., Sprick, R. S., & Dutt, A. (2020). Photocatalytic hydrogen production performance of 1-D ZnO nanostructures: Role of structural properties. *International Journal of Hydrogen Energy*, 45(56), 31942-31951. https://doi.org/10.1016/j.ijhydene.2020.08.247

Georgiou, P., Kolokotronis, K., & Simitzis, J. (2009). Synthesis of ZnO nanostructures by hydrothermal method. *Journal of Nano Research,* 6, 157-168. https://doi.org/10.4028/ www.scientific.net/JNanoR.6.157

Hassanpour, A., Bogdan, N., Capobianco, J. A., & Bianucci, P. (2017). Hydrothermal selective growth of low aspect ratio isolated ZnO nanorods. *Materials and Design,* 119, 464-469. https://doi.org/10.1016/j.matdes.2017.01.089

Hoang, N. H., Nguyen, V. N., & Doan, M. T. (2017). Optimization of an electrode made from CdS–ZnO nanorods for hydrogen generation from photoelectrochemical splitting of water. *Advances in Natural Sciences: Nanoscience and Nanotechnology*, 8(2), Article 025006. https://doi.org/10.1088/2043-6254/aa5e35

Holi, A. M., Zainal, Z., Talib, Z. A., Lim, H.-N., Yap, C.-C., Chang, S.-K., & Ayal, A. K. (2016). Effect of hydrothermal growth time on ZnO nanorod arrays photoelectrode performance. *Optik,* 127(23), 11111-11118. https://doi.org/10.1016/j.ijleo.2016.09.015

Hussain, K., Ahmad, R., Hassan, S., Khan, M. Y., Ahmad, A., Alshammari, M. B., Ali, M. S., Lakho, S. A., & Lee, B.-I. (2024). Electrochemical detection of nalbuphine drug using oval-like ZnO nanostructure -based sensor. *Analytical Biochemistry,* 693, Article 115595. https://doi.org/10.1016/j.ab.2024.115595

Joongpun, P., Feemuchang, K., Onlaor K., Thiwawong, T., & Tunhoo B. (2024). Facile synthesis of zinc oxide nanorods using a single-phase flow with 3d printed device. *Thai Journal of Nanoscience and Nanotechnology*, 9(1), 9-18.

Khan, Z. R., Alshammari, A. S., Bouzidi, M., Shkir, M., & Shukla, D. K. (2021). Improved optoelectronic performance of sol–gel derived ZnO nanostructured thin films. *Inorganic Chemistry Communications,* 132, Article 108812. https://doi.org/10.1016/j.inoche.2021.108812

Kolaei, M., Tayebi, M., Masoumi, Z., & Lee, B.-K. (2022). A novel approach for Improving photoelectrochemical water splitting performance of ZnO-CdS photoanodes: Unveiling the effect of surface roughness of ZnO nanorods on distribution of CdS nanoparticles. *Journal of Alloys and Compounds*, 906, Article 164314. https://doi.org/10.1016/j.jallcom.2022.164314

Kumar, B., & Kim, S.-W. (2012). Energy harvesting based on semiconducting piezoelectric ZnO nanostructures. *Nano Energy,* 1(3), 342-355. https://doi.org/10.1016/j.nanoen.2012. 02.001

Kumari, L., & Kar, A. K. (2018). Tuning the optical properties of ZnO nanorods by variation of precursor concentration through hydrothermal method. *AIP Conference Proceedings*, 1953(1), Article 030158. https://doi.org/10.1063/1.5032493

Lai, Y., Xiao, L., Tao, Y., Gao, Z., Zhang, L., Su, X., & Dai, Y. (2021). Enhancing one-dimensional charge transport in metal-organic framework hexagonal nanorods for electrocatalytic oxygen evolution. *ChemSusChem*, 14(8), 1830-1834. https://doi.org/10.1002/cssc.202100179

Lee, W. C., Fang, Y., Le, H., Hodgson, R., Chan, H. W. B., Qian, R., Alsohaimi, I. H., Canciani, G. E., Alhar, M. S., & Chen, Q. (2024). Enhanced photoelectrochemical water splitting by a 3D hierarchical sea urchin- like structure: ZnO nanorod arrays on TiO2 hollow hemisphere. *Nanotechnology*, 35(29), Article 295301. https://doi.org/10.1088/1361-6528/ad3e88

Leite, R. R., Colombo, R., Júnior, F. E. B., de Vasconcelos Lanza, M. R., da Silva Barud, H., Afonso, C. R. M., & Bernardi, M. I. B. (2024). Precursor effect on the hydrothermal synthesis of pure ZnO nanostructures and enhanced photocatalytic performance for norfloxacin degradation. *Chemical Engineering Journal,* 496, Article 154374. https://doi.org/10.1016/j.cej.2024.154374

Liang, S., Zhu, L., Gai, G., Yao, Y., Huang, J., Ji, X., Zhou, X., Zhang, D., & Zhang, P. (2014). Synthesis of morphology-controlled ZnO microstructures via a microwave-assisted hydrothermal method and their gas-sensing property. *Ultrasonics Sonochemistry*, 21(4), 1335-1342. https://doi.org/10.1016/j.ultsonch.2014.02.007

Mustafa, M. K., Iqbal, Y., Majeed, U., & Sahdan, M. Z. (2017). Effect of precursor's concentration on structure and morphology of ZnO nanorods synthesized through

hydrothermal method on gold surface. *AIP Conference Proceedings,* 1788, Article 030120. https://doi.org/10.1063/1.4968373

Pagano, R., Bettini, S., Ottolini, M., Ciccarella, G., Valli, L., & Giancane, G. (2024). Piezo- and photo- responsive ZnO nanostructures for efficient tetracycline water remediation. *Colloids and Surfaces A: Physicochemical and Engineering Aspects,* 680, Article 132626. https://doi.org/10.1016/j.colsurfa.2023.132626

Palem, R. R., Kim, B. J., Baek, I., Choi, H., Suneetha, M., Shimoga, G., & Lee, S.-H. (2024). In situ fabricated ZnO nanostructures within carboxymethyl cellulose-based ternary hydrogels for wound healing applications. *Carbohydrate Polymers,* 334, Article 122020. https://doi.org/10.1016/j.carbpol.2024.122020

Polsongkram, D., Chamninok, P., Pukird, S., Chow, L., Lupan, O., Chai, G., Khallaf, H., & Schulte, A. (2008). Effect of synthesis conditions on the growth of ZnO nanorods via hydrothermal method. *Physica B: Condensed Matter*, 403(19-20), 3713-3717. https://doi.org/10.1016/j.physb.2008.06.020

Preeti, K., Kumar, A., Jain, N., Kaushik, A., Mishra, Y. K., & Sharma, S. K. (2023). Tailored ZnO nanostructures for efficient sensing of toxic metallic ions of drainage systems. *Materials Today Sustainability,* 24, Article 100515. https://doi.org/10.1016/j.mtsust.2023.100515

Promnimit, S., Baruah, S., Lamdu, U., & Dutta, J. (2013). Hydrothermal growth of ZnO hexagonal nanocrystals: Effect of growth conditions. *Journal of Nano Research*, 21, 57-63. https://doi.org/10.4028/www.scientific.net/JNanoR.21.57

Sha, R., Basak, A., Maity, P. C., & Badhulika, S. (2022). ZnO nano-structured based devices for chemical and optical sensing applications. *Sensors and Actuators Reports,* 4, Article 100098. https://doi.org/10.1016/j.snr.2022.100098

Siriphongsapak, N., Denchitcharoen, S., & Limsuwan, P. (2020). Hydrothermal growth of ZnO nanostructures using sodium hydroxide as a source of hydroxide ion. *Materials Today: Proceedings*, 23(Part 4), 712-719. https://doi.org/10.1016/j.matpr.2019.12.263

Wang, S., Cao, S., Wang, L., Zhan, X., Yang, H., Yang, W., & Hou, H. (2024). Enhanced photoelectrochemistry for energy conversion, environmental remediation, detection, and sensing through single-atom catalysts modified photoelectrodes: a comprehensive review. *Materials Today Energy,* 43, Article 101582. https://doi.org/10.1016/j.mtener.2024.101582

Wasly, H. S., El-Sadek, M. S. A., & Henini, M. (2018). Influence of reaction time and synthesis temperature on the physical properties of ZnO nanoparticles synthesized by the hydrothermal method. *Applied Physics A*, 124, Article 76. https://doi.org/10.1007/s00339-017-1482-4

Wei, R.-B., Kuang, P.-Y., Cheng, H., Chen, Y.-B., Long, J.-Y., Zhang, M.-Y., & Liu, Z.Q. (2017). Plasmon-enhanced photoelectrochemical water splitting on gold nanoparticle decorated ZnO/CdS nanotube arrays. *ACS Sustainable Chemistry and Engineering,* 5(5), 4249-4257. https://doi.org/10.1021/acssuschemeng.7b00242

Worasawat, S., Tasaki, K., Neo, Y., Hatanaka, Y., & Mimura, H. (2019). Vertically aligned ZnO nano-rods and its photo-conductive characteristics related to the catalytic properties. *Thai Journal of Nanoscience and Nanotechnology*, 4(1), 1-11.

Zhang, J., Que, W., Jia, Q., Ye, X., & Ding, Y. (2011). Controllable hydrothermal synthesis of ZnO nanowires arrays on Al-doped ZnO seed layer and patterning of ZnO nanowires arrays via surface modification of substrate. *Applied Surface Science,* 257(23), 10134-10140. https://doi.org/10.1016/j.apsusc.2011.06.163